Carbon-Based Iron Catalysts for Organic Synthesis

Subjects: Chemistry, Organic

Contributor: Fei Wang , Fuying Zhu , Enxiang Ren , Guofu Zhu , Guo-Ping Lu , Yamei Lin

Carbon-based iron catalysts combining the advantages of iron and carbon material are efficient and sustainable catalysts for green organic synthesis.

carbon material iron heterogeneous catalysis organic synthesis

1. Introduction

Organic synthesis has made great contributions to the progress of human society, but has also caused serious environmental pollution [1][2], so there is an urgent demand to introduce green chemistry into this area. One practical tool is the exploration of efficient and selective catalysts for organic synthesis, which can improve synthetic efficiency and reduce production costs and wastes, thereby minimizing the impact on the environment [3][4].

Iron, as the most productive and cheapest metal [5][6][7], is widely available, biocompatible and non-contaminant. The valence state of iron ranges from −2 to +5, which equips it with flexible redox properties, Lewis acidity and coordination ability [8]. Furthermore, iron-based enzymes are involved in lots of vital and efficient transformations *in vivo* [9]. All the above mentioned features of iron render a wonderful candidate to replace noble metals, and stand out among other non-precious metals. Therefore, iron-based catalysts meet the requirement of “catalyst economy”, and the development of these catalysts for organic transformations is conductive to the sustainable development of this area [6]. Nevertheless, the high chemical activity of iron also leads to its poor stability, which limits its application possibilities in more catalytic processes [10][11]. Meanwhile, iron has lower electronegativity and proportion of d orbitals and electrons than noble metals (such as Pd, Ru and Au), so it has poor catalytic activity in hydrogenation and cross-coupling reactions [12][13].

To solve these issues, ligands or supports are required to stabilize or tune the performance of iron sites [14][15][16][17]. Considering that ligands are relatively expensive and non-recyclable, solid supports are undoubtedly more in line with the requirements of green chemistry. Among various supports, carbon materials, with advantages of good biocompatibility, unique microstructure, high specific surface area and excellent physical and chemical properties, are considered excellent supports for iron-based heterogeneous catalysts [18][19][20][21][22][23][24][25]. Therefore, carbon-supported iron materials combining the advantages of iron and carbon materials are an efficient and sustainable catalyst for organic synthesis. In addition, *N*-doped carbon anchored iron-single-atom catalysts have

similar FeN_4 active sites with natural iron-based enzymes in terms of electronic, geometric and chemical structures [26][27].

Although there are several excellent reviews concerning the organic reactions over heterogenous and homogeneous iron-based catalysts [4][5][6][7][8][28][29][30][31][32][33][34][35][36][37], no attempt focuses on the carbon-based iron catalysts for organic synthesis. In recent years, there have been dozens of organic transformations catalyzed by carbon-based iron materials, including oxidation, reduction, tandem and other reactions. Taking into account the advantages and development trends of nanocarbon-based iron catalysts for organic synthesis, the review on this kind of heterogenous catalysts for organic reactions is of great importance and appeal.

2. General Consideration

2.1. The Introduction Strategies of Iron into Carbon Materials

The catalytic activity of carbon-based iron materials is closely related to their structures, which are controlled by their synthetic strategies. Because numerous reviews on carbon-based metal materials have systematically summarized the controlled fabrication of these materials [38][39][40], this research mainly focuses on the introduction methods of iron into carbon materials. There are three main steps for the preparation of these catalysts: precursor synthesis, pyrolysis and post-modification (**Figure 1**). In the precursor synthesis step, iron can be introduced by mechanical mixing, self-assembly and impregnation methods [41][42][43]. Chemical vapor deposition (CVD) can be applied for iron doping during the pyrolysis process [44][45][46]. Impregnation is also an efficient approach for anchoring iron to carbon material in the post-modification step.

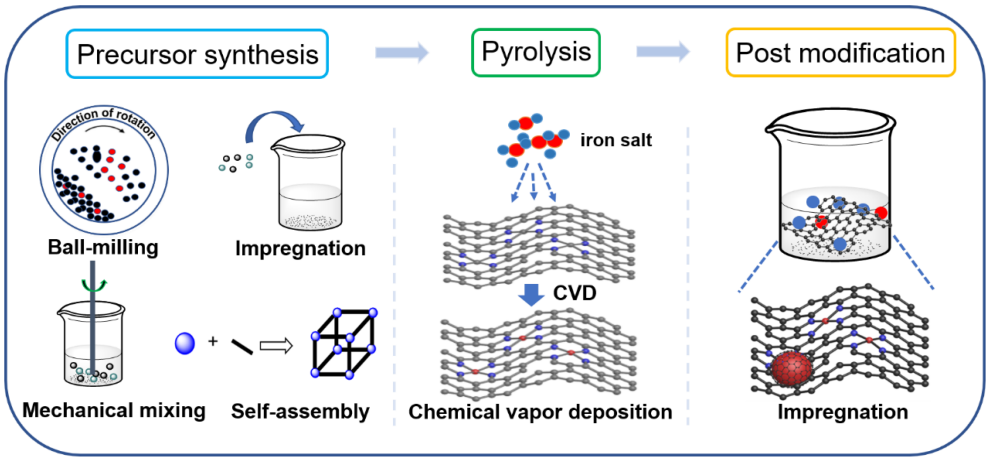

Figure 1. Schematic illustration for the introduction of iron species into carbon supports.

2.1.1. Mechanical Mixing Strategy

Mechanical mixing refers to the direct mixing of iron sources and precursor compounds, without special treatment and requirements on the structure of the precursors. Although this method is easy to be operated, it results in the non-uniformity of carbon particle size and iron distribution [47]. Ball milling has been applied for more even mixing.

In 2015, Deng et al. prepared FeN_4/GN with highly dispersed FeN_4 center by ball milling the mixture of iron phthalocyanine and graphene nanosheets (GNs) [48].

2.1.2. Impregnation Strategy

The impregnation strategy is to impregnate the solution of iron source with carbon materials or carbon precursors, with the removal of residual solvent after impregnation equilibration then leading to the introduction of iron species into carbon materials or carbon precursors [49]. In general, the impregnation method has better mixing efficiency than mechanical mixing, resulting in a more uniform Fe doping. However, the impregnation method still cannot effectively solve the problem on the inhomogeneity of carbon particle size and iron distribution. For example, ethyl cellulose was dissolved in ethanol and mixed with the aqueous solution of $Fe(NO_3)_3{\cdot}9H_2O$, and then melamine and zinc nitrate were added as nitrogen source and pore former, respectively (**Figure 2**a) [50]. However, the size and distribution of carbon and iron particles in Fe@CN-Zn are not uniform, which can be observed from the results of TEM (**Figure 2**b) and SEM (**Figure 2**c).

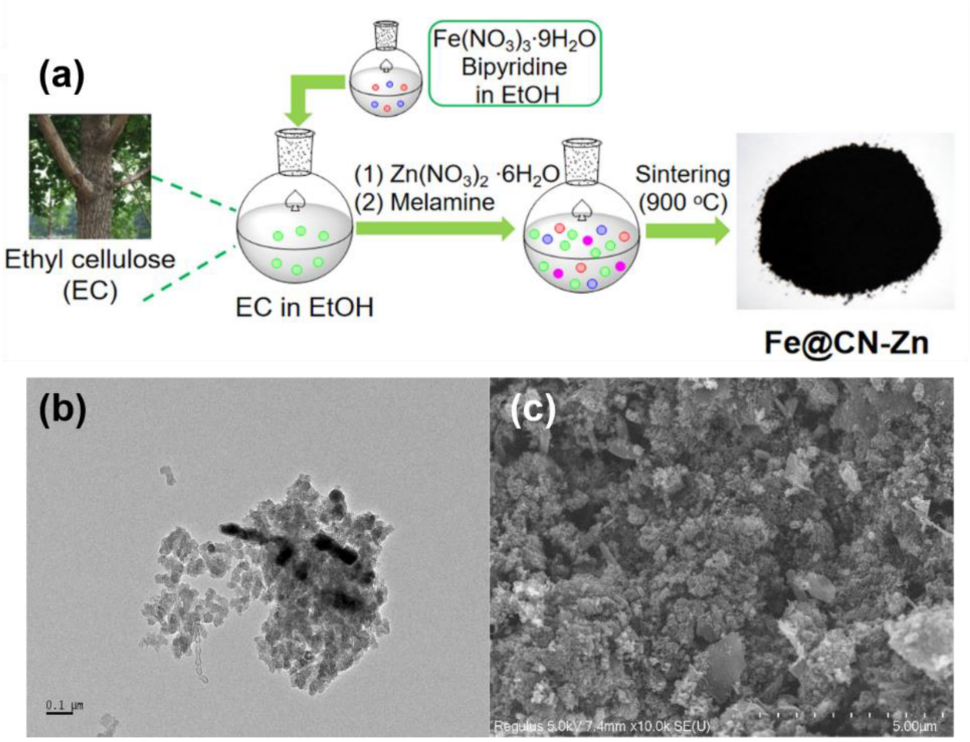

Figure 2. (**a**) Schematic illustration of the synthesis of Fe@CN-Zn. (**b**) TEM and (**c**) SEM images of Fe@CN-Zn. Reprinted with permission from Ref. [50]. Copyright 2021, Elsevier.

2.1.3. Self-Assembly Strategy

The introduction of iron can also be achieved through the self-assembly of iron salts with certain organic ligands to form ordered 3D porous metal-organic frameworks (MOFs), which can be divided into two types: Bimetallic MOFs and Fe-based MOFs. Compared to other methods, nanocarbon-based iron catalysts prepared from self-assembly precursors have advantages of ordered porous structure, more uniform carbon size and iron distribution [51][52][53].

However, this approach has special requirements for organic ligands, which should be able to coordinate with iron ions to form MOFs.

As a bimetallic MOF strategy example, Fe-ZIF (ZIF represents zeolitic imidazolate framework) was prepared via the self-assembly of iron salts and zinc nitrates with 2-methylimidazoles (**Figure 3**a) [43]. An *N*-doped carbon-based iron catalyst was synthesized by the pyrolysis of Fe-ZIF. As a representative example of Fe-based MOF strategy, MIL-101(Fe) was prepared by self-assembly of 1,4-terephthalic acid with iron nitrate hexahydrate, which was grinded with melamine and then calcinated to obtain $Fe/Fe_2O_3@N^nPC$-T-x catalyst (n represents the ratio of MIL-101 (Fe) and melamine, T represents calcination temperature and x represents calcination pyrolysis time) (**Figure 3**b) [54].

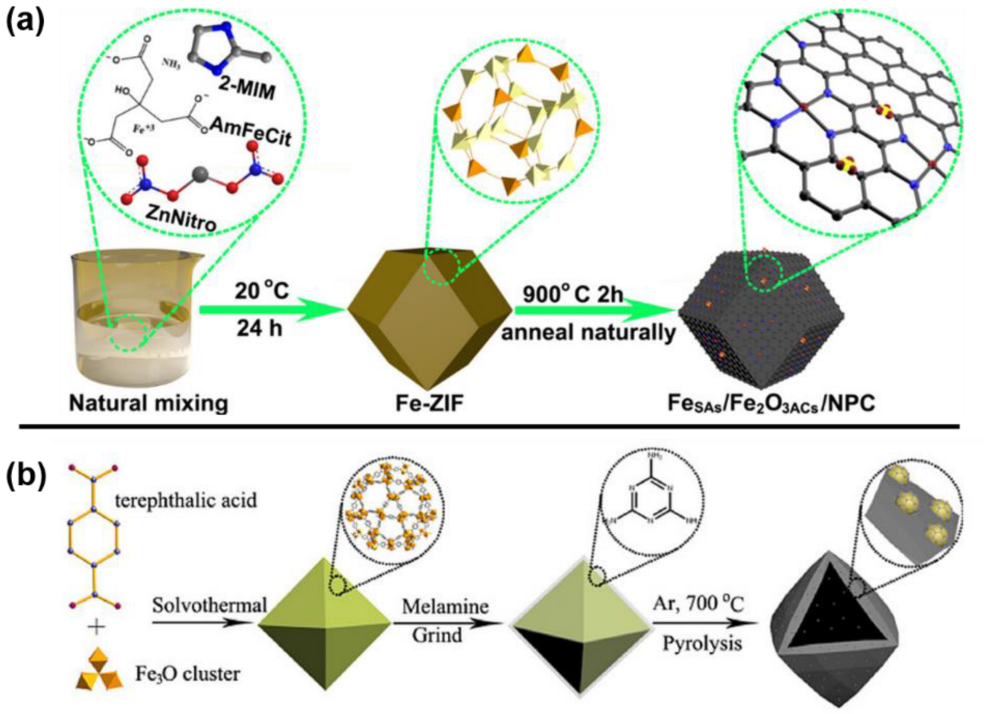

Figure 3. (**a**) The preparation of Fe_{SAs}/Fe_2O_{3ACs}/NPC from bimetallic MOF strategy. Reprinted with permission from Ref. [43]. Copyright 2020, American Chemical Society. (**b**) The preparation of $Fe/Fe_2O_3@N^nPC$-700-x from Fe-based MOF strategy. Reprinted with permission from Ref. [54]. Copyright 2019, Wiley.

2.1.4. Chemical Vapor Deposition (CVD)

Chemical vapor deposition (CVD) refers to a vapor phase self-assembly carbonization process at high temperatures, which can effectively control the chemical composition, morphology, crystal structure and grain size of the membrane layer by adjusting the deposition parameters [55]. This method can make iron species in full contact with the carbon materials during the carbonization process, constructing a unique active iron center, and finally obtaining a catalyst for carbon-loaded iron with excellent catalytic activity. In 2021, Jia et al. prepared a Fe-N-C catalyst containing dense FeN_4 sites by flowing iron vapor through the Zn-N-C substrate at 750 °C (**Figure 4**) [56].

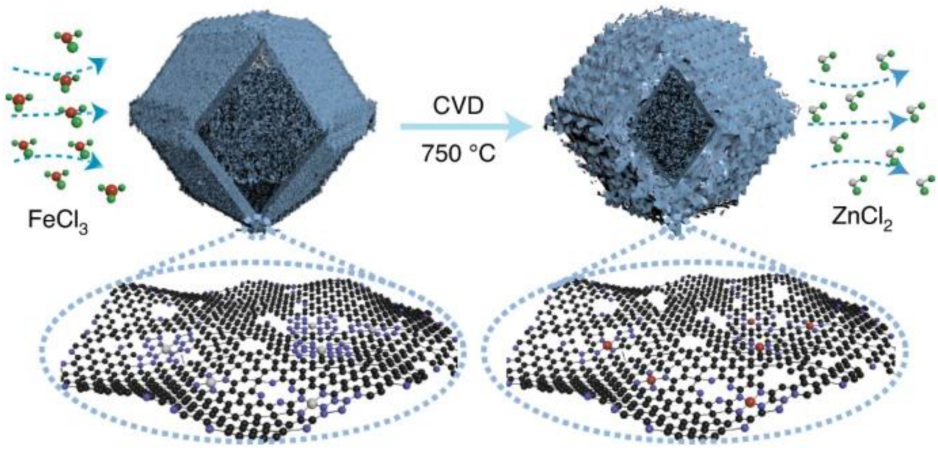

Figure 4. Preparation of FeNC-CVD-750 via CVD strategy. Reprinted with permission from Ref. [56]. Copyright 2021, Springer Nature.

2.2. The Structure and Activity Relationship (SAR)

2.2.1. Nature Properties of the Carbon Materials

In comparison of metal oxide supports, carbon materials have unique porous structure, and are easier to be doped with heteroatoms, which can adjust their Lewis acid-base sites and defect the degree and electronic state of Fe sites, facilitating the formation of stable and active iron catalytic sites. Therefore, iron-doped carbon materials exhibit superior performance than metal oxide-supported iron catalysts in various transformations. For example, Beller's group have prepared two carbon-supported iron catalysts: Fe-phenanthroline/C-800 [57] and Fe-L1@EGO-900 [41], which exhibit good catalytic activity for the reduction of nitroarenes and acceptorless dehydrogenation reactions, respectively. The two catalysts were prepared by calcinating the mixture of iron precursor, 1,10-phenanthroline ligand and carbon support. The difference is that carbon powder was used as carbon support in Fe-phenanthroline/C-800, while exfoliated graphene oxide (EGO) was applied as carbon support in Fe-L1@EGO-900. However, the catalytic efficiency of other heterogeneous iron catalysts is much lower, or even with no catalytic effect when the carbon material is replaced with other carriers, such as Al_2O_3, SiO_2, CeO_2 and TiO_2. Overall, the porous structure and defects of carbon supports are favorable for the interaction between substrates with active sites, as well as the exposure of active sites in the catalysts. The Lewis acid-base sites of carbon supports can improve the adsorption and activation of substrates.

2.2.2. Iron Sites in Carbon Materials

Generally, there are two types of iron sites in carbon materials: single atomic iron sites and iron nanoparticles (NPs) [58][59]. The identification of these two iron sites can be achieved by XRD, TEM, XAFS and HAADF-STEM [60][61][62]. Single atomic iron sites and iron nanoparticles (NPs) can usually play a synergistic catalytic role by exerting their respective catalytic advantages in different steps of one reaction [58][60][63]. Although some control experiments have been designed to verify the synergistic catalytic effect between these two sites, the research on this aspect is still in its infancy.

For example, Yang et al. designed a series of control experiment to confirm the synergistic catalysis on FeN_x sites (single atomic Fe sites) and Fe NPs for the fabrication of quinolones and quinazolinones (**Figure 5**a) [58]. Because acid etching can remove Fe NPs selectively, while SCN^- can specifically poison FeN_x sites, the catalytic effects of FeN_x and Fe NPs in the reaction can be clarified. In addition, the reaction principles of Fe(II)Pc and nano-Fe powder are similar to that of FeN_x sites and Fe NPs, which are also applied to detect the role of FeN_x and Fe NPs during the catalytic process. The coupling reaction of amine and aldehyde and the oxidative dehydrogenation of intermediate I are the two steps involved in the oxidative coupling reaction (**Figure 5**a). As shown in **Figure 5**a, FeN_x sites are more favorable for the formation of intermediate I, while Fe NPs are more conducive to the further dehydrogenation of intermediates I to produce quinolones and quinazolinones. Thus, FeN_x sites and Fe NPs play a synergistic catalytic role in this oxidative coupling reaction.

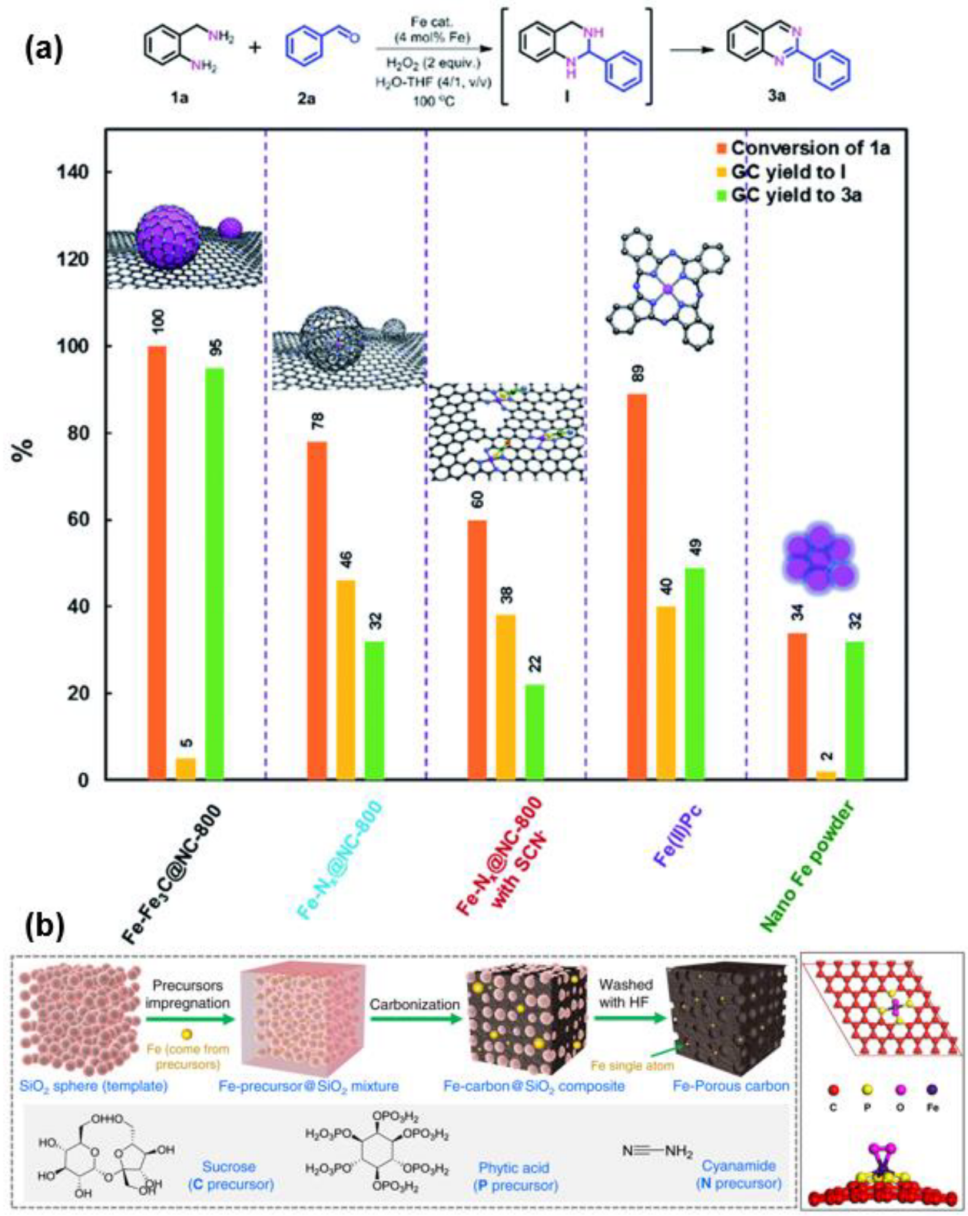

Figure 5. (**a**) The control experiments on the synergistic catalysis between FeN_x sites and Fe NPs. Reprinted with permission from Ref. [58]. Copyright 2019, Royal Society of Chemistry. (**b**) The synthetic route of Fe-P-C. Reprinted

with permission from Ref. [64]. Copyright 2020, Springer Nature.

FeN_x site has similar structure with active sites of natural iron-based enzymes, so it exhibits excellent redox performance under mild conditions. Meanwhile, the coordination environment of iron single-atom sites can also be regulated by manipulating the preparation parameters, such as heteroatom doping, which may further improve the catalytic performance of iron sites. For example, Li et al. prepared phosphorus-doped atomically dispersed catalyst Fe-P-C for the first time, and found that the resulting O_2-Fe-P_4 structure is reduced by hydrogen to generate a large number of Fe-P_4 sites, which is attributed to the excellent catalytic performance of the catalyst in the hydrogenation reaction (**Figure 5**b) [64]. However, the FeN_4 sites generated in Fe-N-C prepared by nitrogen atom doping are less active towards the same reaction.

In general, FeN_x sites have higher atom utilization and catalytic efficiency than iron NPs, while Fe NPs in the catalysts do play a non-negligible catalytic role in many reactions. This is mainly because many organic reactions inherently involve multi-step steps that require the synergy of multiple active sites.

2.2.3. The Construction of SAR

The construction of SAR between carbon-based iron catalysts and organic reactions are mainly explored by control experiments, reaction kinetics studies and density functional theory (DFT). Control experiments are performed to determine possible reaction intermediates and reaction pathways by changing the reaction conditions or substrates appropriately, or by adding additives. As shown in Scheme 1, the role of Fe-Fe_3C@NC-800 and H_2O_2 in the reaction is investigated by control experiments. Based on the results of Scheme 1, it can be concluded that Fe-Fe_3C@NC-800 is necessary for both the coupling and dehydrogenation process, while H_2O_2 is favorable for the dehydrogenation process [58].

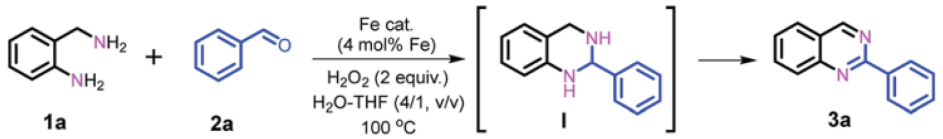

Entry	Deviation from standard conditions	Conversion (%)	GC yield (%)	
			I	**3a**
1	none	100	5	95
2	in the absence of H_2O_2	100	90	10
3	FePc as catalyst instead	65	62	3
4	in the absence of catalyst	15	15	0

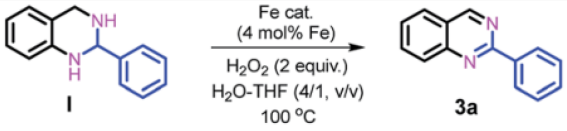

Entry	Deviation from standard conditions	**3a** GC yield (%)
5	none	99
6	in the absence of H_2O_2	12
7	in the absence of catalyst	10

Scheme 1. The role of Fe-Fe_3C@NC-800 and H_2O_2 in mechanism exploration. Reprinted with permission from Ref. [58]. Copyright 2019, Royal Society of Chemistry.

The main purpose of reaction kinetic studies is to determine the rate-determining step (RDS) of the reaction. RDS is the most critical step in the complex organic reactions, so determining RDS is beneficial to simplify the studies of the reaction mechanism. Kinetic isotope experiments (KIE) is a commonly used approach to determine RDS, in which the k_H/k_D value can be an indicator for RDS [65]. The RDS can also be determined by detecting reaction orders, which reflects the effect of reactant concentration on the reaction rate. For example, the group determines the borrowing hydrogen *N*-alkylation reaction order of benzyl alcohol and benzylamine, and performs KIE to confirm the RDS (**Figure 6**) [66]. The reaction order of aniline in this reaction is negative, while that of benzyl alcohol is positive (**Figure 6**b,c), confirming the activation of benzyl alcohol may be involved in the RDS [67]. The parallel experiments are performed by using $PhCH_2OH$ and isotope-labeled $PhCD_2OH$ to go through this reaction respectively, and the k_H/k_D of this reaction is calculated to be 2.75 (**Figure 6**a), further indicating that the C-H activation of benzyl alcohol may be related to RDS.

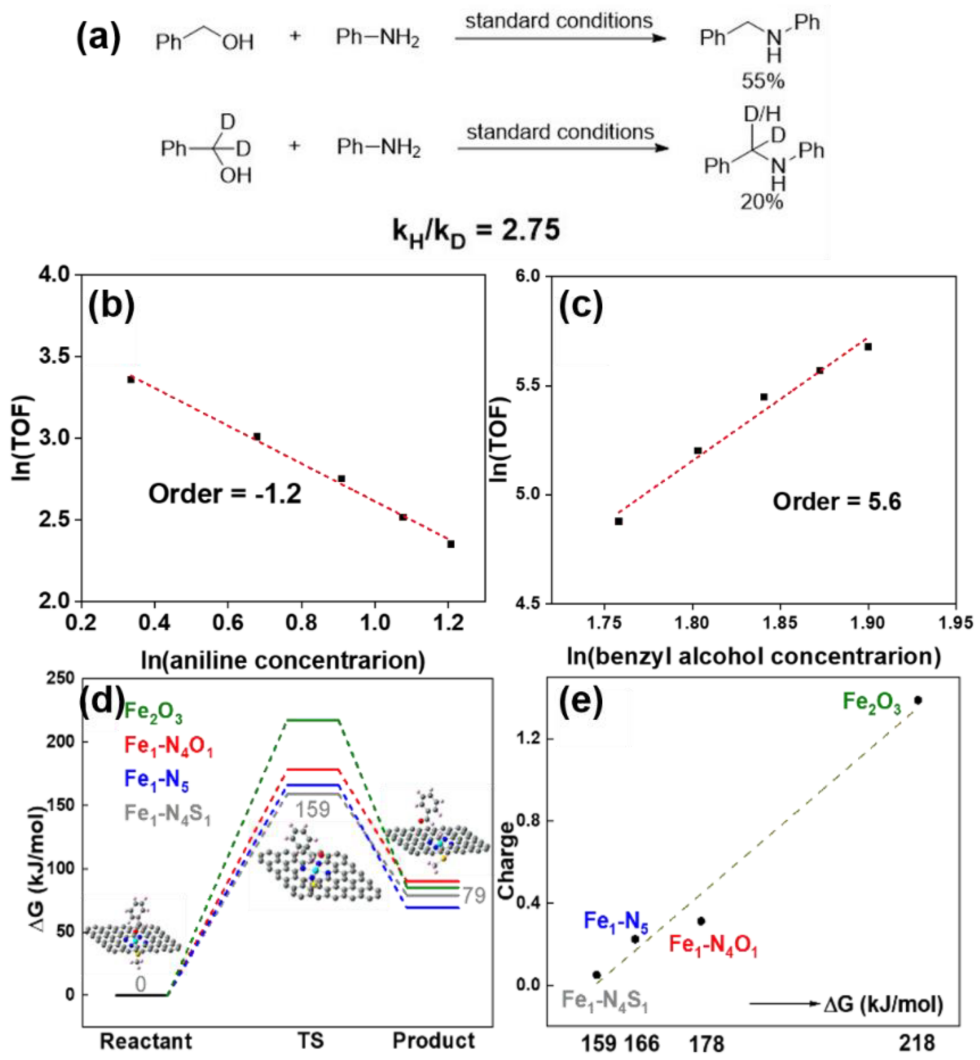

Figure 6. (**a**) The H/D kinetic isotope effect (KIE) experiment results. Plots of reaction orders of (**b**) aniline and (**c**) benzyl alcohol. (**d**) The energy barriers for Fe_2O_3, Fe_1-N_4O_1, Fe_1-N_5 and Fe_1-N_4S_1 sites. (**e**) The relationship between positive charge density of Fe sites and energy barriers. Reprinted with permission from Ref. [66]. Copyright 2021, Royal Society of Chemistry.

In addition, DFT calculations can further confirm the main catalytic active center in RDS by comparing the energy barriers, which can also provide useful information for the construction of SAR between carbon-based iron catalysts and organic reactions. For instance, to further identify the catalytically active center, the RDS energy barriers of different Fe sites can be calculated based on DFT [4][43][68][69][70]. The energy barriers of these four sites can be sorted as Fe_1-N_4S_1 < Fe_1-N_5 < Fe_1-N_4O_1 < Fe_2O_3, which are positively related to their positive charge density (**Figure 6**d,e). These results suggest that Fe_1-N_4S_1 and Fe_1-N_5 are more likely to be the main catalytically active sites for the RDS process [66].

Based on these results, a possible strategy for construction the structure-activity relationship is listed: (1) confirming the rate-determining steps of reactions and the main active sites of carbon-based iron catalysts by

catalyst characterization data, control and kinetic experiments; and (2) establishing the relationship between the two based on reaction yields and structural information of the active sites, and confirming it by DFT calculations.

References

1. Rodionov, I.A.; Zvereva, I.A. Photocatalytic activity of layered perovskite-like oxides in practically valuable chemical reactions. Russ. Chem. Rev. 2016, 85, 248–279.
2. Ju, S.; Shin, G.; Lee, M.; Koo, J.M.; Jeon, H.; Ok, Y.S.; Hwang, D.S.; Hwang, S.Y.; Oh, D.X.; Park, J. Biodegradable chito-beads replacing non-biodegradable microplastics for cosmetics. Green Chem. 2021, 23, 6953–6965.
3. Rydel-Ciszek, K.; Pacześniak, T.; Zaborniak, I.; Błoniarz, P.; Surmacz, K.; Sobkowiak, A.; Chmielarz, P. Iron-Based Catalytically Active Complexes in Preparation of Functional Materials. Processes 2020, 8, 1683.
4. Shesterkina, A.A.; Kustov, L.M.; Strekalova, A.A.; Kazansky, V.B. Heterogeneous iron-containing nanocatalysts—Promising systems for selective hydrogenation and hydrogenolysis. Catal. Sci. Technol. 2020, 10, 3160–3174.
5. Shang, R.; Ilies, L.; Nakamura, E. Iron-Catalyzed C-H Bond Activation. Chem. Rev. 2017, 117, 9086–9139.
6. Furstner, A. Iron Catalysis in Organic Synthesis: A Critical Assessment of What It Takes to Make This Base Metal a Multitasking Champion. ACS Cent. Sci. 2016, 2, 778–789.
7. Wei, D.; Darcel, C. Iron Catalysis in Reduction and Hydrometalation Reactions. Chem. Rev. 2019, 119, 2550–2610.
8. Bauer, I.; Knolker, H.J. Iron catalysis in organic synthesis. Chem. Rev. 2015, 115, 3170–3387.
9. Bertini, I.; Gray, H.B.; Lippard, S.J.; Valentine, J.S. Bioinorganic Chemistry; University Science Books: Mill Valley, CA, USA, 1994.
10. Wang, Q.; Tao, H.L.; Li, Z.Q.; Wang, G.X. Effect of iron precursor on the activity and stability of PtFe/C catalyst for oxygen reduction reaction. J. Alloy Compd. 2020, 814, 152212.
11. Wu, Q.S.; Yang, H.P.; Kang, L.; Gao, Z.; Ren, F.F. Fe-based metal-organic frameworks as Fenton-like catalysts for highly efficient degradation of tetracycline hydrochloride over a wide pH range: Acceleration of Fe (II)/Fe (III) cycle under visible light irradiation. Appl. Catal. B-Environ. 2020, 263, 118282.
12. Hedstrom, A.; Lindstedt, E.; Norrby, P.O. On the oxidation state of iron in iron-mediated C-C couplings. J. Organomet. Chem. 2013, 748, 51–55.

13. Sun, X.B.; Hansen, T.; Poater, J.; Hamlin, T.A.; Bickelhaupt, F.M. Rational design of iron catalysts for C-X bond activation. J. Comput. Chem. 2022, in press.
14. Zuo, W.W.; Lough, A.J.; Li, Y.F.; Morris, R.H. Amine(imine)diphosphine Iron Catalysts for Asymmetric Transfer Hydrogenation of Ketones and Imines. Science 2013, 342, 1080–1083.
15. Morris, R.H. Exploiting Metal-Ligand Bifunctional Reactions in the Design of Iron Asymmetric Hydrogenation Catalysts. Accounts Chem. Res. 2015, 48, 1494–1502.
16. Raji, M.; Mirbagheri, S.A.; Ye, F.; Dutta, J. Nano zero-valent iron on activated carbon cloth support as Fenton-like catalyst for efficient color and COD removal from melanoidin wastewater. Chemosphere 2021, 263, 127945.
17. Cui, X.J.; Li, Y.H.; Bachmann, S.; Scalone, M.; Surkus, A.E.; Junge, K.; Topf, C.; Beller, M. Synthesis and Characterization of Iron-Nitrogen-Doped Graphene/Core-Shell Catalysts: Efficient Oxidative Dehydrogenation of N-Heterocycles. J. Am. Chem. Soc. 2015, 137, 10652–10658.
18. Varma, R.S. Biomass-Derived Renewable Carbonaceous Materials for Sustainable Chemical and Environmental Applications. ACS Sustain. Chem. Eng. 2019, 7, 6458–6470.
19. Kramer, S.; Hejjo, F.; Rasmussen, K.H.; Kegnæs, S. Silylative Pinacol Coupling Catalyzed by Nitrogen-Doped Carbon-Encapsulated Nickel/Cobalt Nanoparticles: Evidence for a Silyl Radical Pathway. ACS Catal. 2017, 8, 754–759.
20. Lin, Y.; Yu, J.; Zhang, X.; Fang, J.; Lu, G.-P.; Huang, H. Carbohydrate-derived porous carbon materials: An ideal platform for green organic synthesis. Chin. Chem. Lett. 2022, 33, 186–196.
21. Sun, K.; Shan, H.; Lu, G.P.; Cai, C.; Beller, M. Synthesis of N-Heterocycles via Oxidant-Free Dehydrocyclization of Alcohols Using Heterogeneous Catalysts. Angew. Chem. Int. Ed. Engl. 2021, 60, 25188–25202.
22. Lam, E.; Luong, J.H.T. Carbon Materials as Catalyst Supports and Catalysts in the Transformation of Biomass to Fuels and Chemicals. ACS Catal. 2014, 4, 3393–3410.
23. Borchardt, L.; Zhu, Q.-L.; Casco, M.E.; Berger, R.; Zhuang, X.; Kaskel, S.; Feng, X.; Xu, Q. Toward a molecular design of porous carbon materials. Mater. Today 2017, 20, 592–610.
24. Sun, K.; Shan, H.; Ma, R.; Wang, P.; Neumann, H.; Lu, G.P.; Beller, M. Catalytic oxidative dehydrogenation of N-heterocycles with nitrogen/phosphorus co-doped porous carbon materials. Chem. Sci. 2022, 13, 6865–6872.
25. Su, T.Y.; Lu, G.P.; Sun, K.K.; Zhang, M.; Cai, C. ZIF-derived metal/N-doped porous carbon nanocomposites: Efficient catalysts for organic transformations. Catal. Sci. Technol. 2022, 12, 2106–2121.
26. Jiao, L.; Yan, H.; Wu, Y.; Gu, W.; Zhu, C.; Du, D.; Lin, Y. When Nanozymes Meet Single-Atom Catalysis. Angew. Chem. Int. Ed. Engl. 2020, 59, 2565–2576.

27. Lin, Y.; Wang, F.; Yu, J.; Zhang, X.; Lu, G.-P. Iron single-atom anchored N-doped carbon as a ‘laccase-like’ nanozyme for the degradation and detection of phenolic pollutants and adrenaline. J. Hazard. Mater. 2021, 425, 127763.
28. Rana, S.; Biswas, J.P.; Paul, S.; Paik, A.; Maiti, D. Organic synthesis with the most abundant transition metal-iron: From rust to multitasking catalysts. Chem. Soc. Rev. 2021, 50, 243–472.
29. Wang, X.; Zhang, X.; Zhang, Y.; Wang, Y.; Sun, S.-P.; Wu, W.D.; Wu, Z. Nanostructured semiconductor supported iron catalysts for heterogeneous photo-Fenton oxidation: A review. J. Mater. Chem. A 2020, 8, 15513–15546.
30. Raya-Barón, Á.; Oña-Burgos, P.; Fernández, I. Iron-Catalyzed Homogeneous Hydrosilylation of Ketones and Aldehydes: Advances and Mechanistic Perspective. ACS Catal. 2019, 9, 5400–5417.
31. Balaraman, E.; Nandakumar, A.; Jaiswal, G.; Sahoo, M.K. Iron-catalyzed dehydrogenation reactions and their applications in sustainable energy and catalysis. Catal. Sci. Technol. 2017, 7, 3177–3195.
32. Damiano, C.; Sonzini, P.; Gallo, E. Iron catalysts with N-ligands for carbene transfer of diazo reagents. Chem. Soc. Rev. 2020, 49, 4867–4905.
33. Batista, V.F.; Pinto, D.C.G.A.; Silva, A.M.S. Iron: A Worthy Contender in Metal Carbene Chemistry. ACS Catal. 2020, 10, 10096–10116.
34. Sears, J.D.; Neate, P.G.N.; Neidig, M.L. Intermediates and Mechanism in Iron-Catalyzed Cross-Coupling. J. Am. Chem. Soc. 2018, 140, 11872–11883.
35. Bakas, N.J.; Neidig, M.L. Additive and Counterion Effects in Iron-Catalyzed Reactions Relevant to C-C Bond Formation. ACS Catal. 2021, 11, 8493–8503.
36. Cassani, C.; Bergonzini, G.; Wallentin, C.-J. Active Species and Mechanistic Pathways in Iron-Catalyzed C-C Bond-Forming Cross-Coupling Reactions. ACS Catal. 2016, 6, 1640–1648.
37. Bailly, B.; Thomas, S.P. Iron-catalysed reduction of carbonyls and olefins. RSC Adv. 2011, 1, 1435–1445.
38. Liu, P.; Gao, S.; Wang, Y.; Huang, Y.; He, W.; Huang, W.; Luo, J. Carbon nanocages with N-doped carbon inner shell and Co/N-doped carbon outer shell as electromagnetic wave absorption materials. Chem. Eng. J. 2020, 381, 122653.
39. Yang, L.Y.; Feng, Y.; Yu, D.B.; Qiu, J.H.; Zhang, X.F.; Dong, D.H.; Yao, J.F. Design of ZIF-based CNTs wrapped porous carbon with hierarchical pores as electrode materials for supercapacitors. J. Phys. Chem. Solids 2019, 125, 57–63.
40. Zhang, X.; Fan, Q.Y.; Yang, H.; Xiao, H.Y.; Xiao, Y.H. Metal-organic framework assisted synthesis of nitrogen-doped hollow carbon materials for enhanced supercapacitor performance. New J. Chem. 2018, 42, 17389–17395.

41. Jaiswal, G.; Landge, V.G.; Jagadeesan, D.; Balaraman, E. Iron-based nanocatalyst for the acceptorless dehydrogenation reactions. Nat. Commun. 2017, 8, 2147–2159.
42. Jagadeesh, R.V.; Stemmler, T.; Surkus, A.-E.; Junge, H.; Junge, K.; Beller, M. Hydrogenation using iron oxide-based nanocatalysts for the synthesis of amines. Nat. Protoc. 2015, 10, 548–557.
43. Yun, R.; Zhan, F.; Li, N.; Zhang, B.; Ma, W.; Hong, L.; Sheng, T.; Du, L.; Zheng, B.; Liu, S. Fe Single Atoms and Fe2O3 Clusters Liberated from N-Doped Polyhedral Carbon for Chemoselective Hydrogenation under Mild Conditions. ACS Appl. Mater. Inter. 2020, 12, 34122–34129.
44. Li, J.K.; Jiao, L.; Wegener, E.; Richard, L.L.; Liu, E.S.; Zitolo, A.; Sougrati, M.T.; Mukerjee, S.; Zhao, Z.P.; Huang, Y.; et al. Evolution Pathway from Iron Compounds to Fe-1(II)-N-4 Sites through Gas-Phase Iron during Pyrolysis. J. Am. Chem. Soc. 2020, 142, 1417–1423.
45. Deng, B.; Liu, Z.; Peng, H. Toward Mass Production of CVD Graphene Films. Adv. Mater. 2019, 31, 1800996.
46. Wang, J.B.; Ren, Z.; Hou, Y.; Yan, X.L.; Liu, P.Z.; Zhang, H.; Zhang, H.X.; Guo, J.J. A review of graphene synthesis at low temperatures by CVD methods. New Carbon Mater. 2020, 35, 193–208.
47. Amadi, E.V.; Venkataraman, A.; Papadopoulos, C. Nanoscale self-assembly: Concepts, applications and challenges. Nanotechnology 2022, 33, 1361–6528.
48. Deng, D.; Chen, X.; Yu, L.; Wu, X.; Liu, Q.; Liu, Y.; Yang, H.; Tian, H.; Hu, Y.; Du, P.; et al. A single iron site confined in a graphene matrix for the catalytic oxidation of benzene at room temperature. Sci. Adv. 2015, 1, e1500462.
49. Guayaquil-Sosa, J.F.; Calzada, A.; Serrano, B.; Escobedo, S.; de Lasa, H. Hydrogen Production via Water Dissociation Using Pt-TiO2 Photocatalysts: An Oxidation-Reduction Network. Catalysts 2017, 7, 324.
50. Lin, Y.; Wang, F.; Lu, G.-P.; Zhang, X. Ethyl cellulose derived porous N-doped carbon material for N-H carbene insertion reaction. Tetrahedron 2021, 98, 132432.
51. Song, C.; Wang, Z.G.; Ding, B.Q. Smart Nanomachines Based on DNA Self-Assembly. Small 2013, 9, 2382–2392.
52. Boal, A.K.; Ilhan, F.; DeRouchey, J.E.; Thurn-Albrecht, T.; Russell, T.P.; Rotello, V.M. Self-assembly of nanoparticles into structured spherical and network aggregates. Nature 2000, 404, 746–748.
53. Whitesides, G.M.; Grzybowski, B. Self-assembly at all scales. Science 2002, 295, 2418–2421.

54. Yun, R.R.; Hong, L.R.; Ma, W.J.; Jia, W.G.; Liu, S.J.; Zheng, B.S. Fe/Fe2O3@N-dopped Porous Carbon: A High-Performance Catalyst for Selective Hydrogenation of Nitro Compounds. ChemCatChem 2019, 11, 724–728.
55. Tsen, A.W.; Brown, L.; Levendorf, M.P.; Ghahari, F.; Huang, P.Y.; Havener, R.W.; Ruiz-Vargas, C.S.; Muller, D.A.; Kim, P.; Park, J. Tailoring Electrical Transport Across Grain Boundaries in Polycrystalline Graphene. Science 2012, 336, 1143–1146.
56. Jiao, L.; Li, J.K.; Richard, L.L.; Sun, Q.; Stracensky, T.; Liu, E.R.; Sougrati, M.T.; Zhao, Z.P.; Yang, F.; Zhong, S.C.; et al. Chemical vapour deposition of Fe-N-C oxygen reduction catalysts with full utilization of dense Fe-N4 sites. Nat. Mater. 2021, 20, 1385–1391.
57. Jagadeesh, R.V.; Surkus, A.E.; Junge, H.; Pohl, M.M.; Radnik, J.; Rabeah, J.; Huan, H.M.; Schunemann, V.; Bruckner, A.; Beller, M. Nanoscale Fe2O3-Based Catalysts for Selective Hydrogenation of Nitroarenes to Anilines. Science 2013, 342, 1073–1076.
58. Ma, Z.; Song, T.; Yuan, Y.; Yang, Y. Synergistic catalysis on Fe-Nx sites and Fe nanoparticles for efficient synthesis of quinolines and quinazolinones via oxidative coupling of amines and aldehydes. Chem. Sci. 2019, 10, 10283–10289.
59. Rui, T.; Lu, G.-P.; Zhao, X.; Cao, X.; Chen, Z. The synergistic catalysis on Co nanoparticles and CoNx sites of aniline-modified ZIF derived for oxidative esterification of HMF. Chinese Chem. Lett. 2021, 32, 685–690.
60. Liu, W.; Zhang, L.; Liu, X.; Liu, X.; Yang, X.; Miao, S.; Wang, W.; Wang, A.; Zhang, T. Discriminating Catalytically Active FeNx Species of Atomically Dispersed Fe-N-C Catalyst for Selective Oxidation of the C-H Bond. J. Am. Chem. Soc. 2017, 139, 10790–10798.
61. Liu, J.; Zou, Y.; Cruz, D.; Savateev, A.; Vilé, G. Ligand-Metal Charge Transfer Induced via Adjustment of Textural Properties Controls the Performance of Single-Atom Catalysts during Photocatalytic Degradation. ACS Appl. Mater. Inter. 2021, 13, 25858–25867.
62. Ding, S.; Lyu, Z.; Zhong, H.; Liu, D.; Sarnello, E.; Fang, L.; Xu, M.; Engelhard, M.H.; Tian, H.; Li, T.; et al. An Ion-Imprinting Derived Strategy to Synthesize Single-Atom Iron Electrocatalysts for Oxygen Reduction. Small 2021, 17, e2004454.
63. Jiang, W.J.; Gu, L.; Li, L.; Zhang, Y.; Zhang, X.; Zhang, L.J.; Wang, J.Q.; Hu, J.S.; Wei, Z.; Wan, L.J. Understanding the High Activity of Fe-N-C Electrocatalysts in Oxygen Reduction: Fe/Fe3C Nanoparticles Boost the Activity of Fe-Nx. J. Am. Chem. Soc. 2016, 138, 3570–3578.
64. Long, X.; Li, Z.; Gao, G.; Sun, P.; Wang, J.; Zhang, B.; Zhong, J.; Jiang, Z.; Li, F. Graphitic phosphorus coordinated single Fe atoms for hydrogenative transformations. Nat. Commun. 2020, 11, 4074.
65. Wang, H.; Xu, D.; Guan, E.; Wang, L.; Zhang, J.; Wang, C.; Wang, S.; Xu, H.; Meng, X.; Yang, B.; et al. Atomically Dispersed Ru on Manganese Oxide Catalyst Boosts Oxidative Cyanation. ACS

Catal. 2020, 10, 6299–6308.

66. Lu, G.P.; Shan, H.B.; Lin, Y.M.; Zhang, K.; Zhou, B.J.; Zhong, Q.; Wang, P.C. A Fe single atom on N, S-doped carbon catalyst for performing N-alkylation of aromatic amines under solvent-free conditions. J. Mater. Chem. A 2021, 9, 25128–25135.
67. Wang, Y.; Furukawa, S.; Yan, N. Identification of an Active NiCu Catalyst for Nitrile Synthesis from Alcohol. ACS Catal. 2019, 9, 6681–6691.
68. Li, J.; Sun, H.; Liu, J.-X.; Zhang, J.-J.; Li, Z.-X.; Fu, Y. Selective reductive cleavage of CO bond in lignin model compounds over nitrogen-doped carbon-supported iron catalysts. Mol. Catal. 2018, 452, 36–45.
69. Yun, R.; Zhang, S.; Ma, W.; Lv, X.; Liu, S.; Sheng, T.; Wang, S. Fe/Fe3C Encapsulated in N-Doped Carbon Tubes: A Recyclable Catalyst for Hydrogenation with High Selectivity. Inorg. Chem. 2019, 58, 9469–9475.
70. Cheong, W.C.; Yang, W.J.; Zhang, J.; Li, Y.; Zhao, D.; Liu, S.J.; Wu, K.L.; Liu, Q.G.; Zhang, C.; Wang, D.S.; et al. Isolated Iron Single-Atomic Site-Catalyzed Chemoselective Transfer Hydrogenation of Nitroarenes to Arylamines. ACS Appl. Mater. Inter. 2019, 11, 33819–33824.